Proceedings of the 52nd ISCIE International Symposium
on Stochastic Systems Theory and Its Applications
Osaka, Oct. 29-30, 2020

Three degree-of-freedom stochastic modeling of human-bicycle balance fluctuations

Mikinori Ito, Hayate Kaido, Yoshikazu Yamanaka, and Katsutoshi Yoshida

Department of Mechanical Systems Engineering, Utsunomiya University
7-1-2 Yoto, Utsunomiya, Tochigi 321-8585, Japan
E-mail: {ito,kaido}@katzlab.jp, {yyamanaka,yoshidak}@cc.utsunomiya-u.ac.jp

Abstract

In this study, we propose a new three degree-of-freedom (DOF) fluctuation model that accurately reproduces the probability density functions (PDFs) of human-bicycle balance motions as simply as possible. First, we measure the PDFs of the roll angular displacement, wheel's lateral displacement, steering angular displacement, and each velocity. Next, using these PDFs as training data, we identify the model parameters by means of particle swarm optimization (PSO); in particular, we minimize the squared residuals between the experimental PDFs from the participants and our simulated PDFs. The resulting PDF fitnesses were over 97% for all participants, indicating that our simulated PDFs reproduced the human PDFs.

1 Introduction

Bicycles provide a useful means of short-distance transportation and their utilization is expected to contribute to building a healthy and environmentally friendly society. However, bicycle transportation is not always safe due to collisions with automobiles [1].

To avoid such accidents by means of autonomous vehicle technology, accurate simulation models of bicycle motions are required. Bicycle motions in traffic seem to be classified into two types: voluntary and involuntary. The former comprises purposeful motions such as right and left turning at a street intersection, which motions have been investigated by Google [2]. The latter comprises unconscious motions such as human fluctuated balance motions, which have already been found universally in human quiet standing [3], human stick balancing [4], visuomotor tracking [5], and so on.

In this study, we investigate the latter type of bicycle motion, i.e., involuntary human-bicycle motions, by proposing a new three DOF stochastic model that accurately reproduces the PDFs of them with respect to their roll angular displacement, wheel's lateral displacement, steering angular displacement, and each velocity. This model provides a larger DOF extension to our previous single DOF model [6] with respect to the roll angle only and is expected to provide a key technology for simulating the bicycle running paths. To this end, we have conducted an experiment in which each human participant rides a bicycle on bicycle-trainer rollers, allowing it to move without rolling or yawing constraints. During this experiment, we measured the PDFs of the bicycle roll angular displacement, wheel's lateral displacement, steering angular displacement, and each velocity. We designed our proposed human-bicycle model as a carted inverted pendulum mechanism controlled by our human controller model, which was successfully used in our previous studies [5, 6]. The model parameters were identified based on the measured PDFs as training data, using PSO to minimize the squared residuals (SRs) between the measured and simulated PDFs. The results show that our proposed model successfully reproduces the measured PDFs with SR fitnesses of over 97%.

Our proposed approach mentioned above sharply contrasts with other studies in the fields of autonomous or unmanned bicycle-control systems [7, 8] and also with Google's study on voluntary bicycle motions [2]. Another study on stochastic modeling of bicycle fluctuated motion [9] can be found; however, it addressed the large-scale bicycle running paths, unlike our study.

The rest of the paper is structured as follows: Section 2 describes the human-bicycle experiment. Section 3 describes our proposed stochastic model. Sections 4 and 5 describe our parameter identification method and results. Section 6 concludes our study.

2 Human-bicycle balance experiment

2.1 Experimental setup and procedure

Figure 1 shows a photograph of our experimental device and a participant. The experimental device consists of five units: a bicycle (BE-ELL03, Panasonic, Japan), a set of bicycle-trainer rollers (E-MOTION, Elite, Italy), a set of motion capture cameras (GV500, Library, Japan), a three-dimensional measurement software (Move-tr/3D, Library, Japan), and a computer.

The experimental participants were three healthy males in their early twenties. They were first instructed on the operation of the experimental device, the number of trials, and the duration of each trial. The experiment was performed according to the principles of the Declaration of Helsinki and informed consent was obtained.

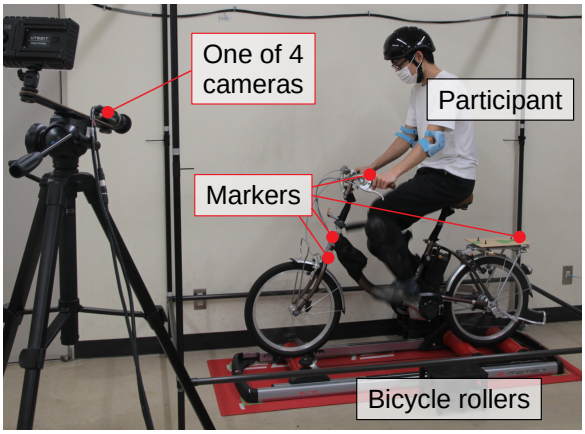

Fig. 1: Photograph of our experimental device, a human participant.

In each trial, the participant rode the bicycle on the trainer rollers for significantly more than 257 s at a speed about 12 km/h. Several practice trials were performed prior to measurement. The air pressure was set to 680 kPa.

2.2 Experimental data

During each trial, the time series of the measurement vector,

$$\begin{aligned}\boldsymbol{x}(t) &= (x_1(t), \cdots, x_6(t))^T \\ &:= (\theta(t), \dot{\theta}(t), y(t), \dot{y}(t), \phi(t), \dot{\phi}(t))^T \end{aligned} \quad (1)$$

(hereafter, $(\cdot)^T$ denotes a transpose), was obtained by the motion capture cameras and software. Here, θ [rad] is the roll angle from the vertical line to the bicycle's vertical axis and $\dot{\theta} := d\theta/dt$ [rad/s] is the corresponding angular velocity, y [m] is the wheel's lateral displacement, $\dot{y} := dy/dt$ [m/s] is the corresponding wheel's lateral velocity, ϕ [rad] is the steering angle from the longitudinal axis to the bicycle's longitudinal axis, and $\dot{\phi} := d\phi/dt$ [rad/s] is the corresponding angular velocity. Figure 2 schematically shows the definition of the roll angle θ in the front view of the bicycle. Figure 3 schematically shows the definition of the wheel's lateral displacement y and the steering angle ϕ in the top view of the bicycle front wheel. The bicycle's vertical and longitudinal axes were nominally determined based on the direction of the bicycle frame and the bicycle handle stem, respectively. The axis of the lateral wheel's displacement were nominally determined based on the direction of the rotation axis of the bicycle-trainer's front roller.

Note that, in our experiment, the rotational origins $\theta = 0$ and $\phi = 0$ were calibrated to fit the bicycle's vertical parking position; therefore, these do not indicate, respectively, the physical upright equilibrium and the physical straight running position of the unmanned bicycle. In addition, the wheel's lateral origin $y = 0$ does not indicate vibrational center of y; the center depends on the human riding motions.

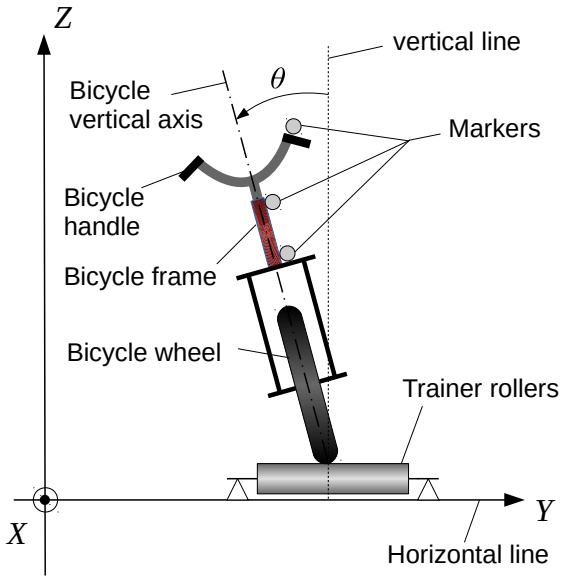

Fig the exp

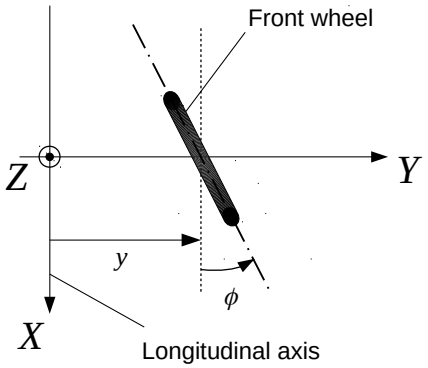

Fig. 3: Schematic top view of the bicycle front wheel during the experiment.

Throughout the experiment, $\boldsymbol{x}(t)$ were stored in the computer in the following form:

$$\begin{aligned}&\{\boldsymbol{x}_{hum}^{(s,n)}(t_0), \cdots, \boldsymbol{x}_{hum}^{(s,n)}(t_i), \cdots, \boldsymbol{x}_{hum}^{(s,n)}(t_{I-1})\}, \\ &\quad i = 0, \cdots, I-1,\ s = 1, \cdots, S,\ n = 1, \cdots, N, \end{aligned} \quad (2)$$

where $t_i := i\Delta t$ [s] is a discrete time with a sampling period of Δt, I is the length of the time series, s and S are an index and the number of participants, respectively, and n and N are an index and the number of trials, respectively.

For this study, we chose $\Delta t = 1/70$ s and $I = 18001$ for the physical data length $(I-1)\Delta t = 258$ s. The number of participants was $S = 3$ and the number of trials undertaken by each participant was $N = 5$.

2.3 Construction of measured PDFs

We obtain $P_{hum}^{(s,n)}(x_k)$, the PDF with respect to the kth component of the time series in (2) for the sth participant's nth trial, by normalizing the histogram

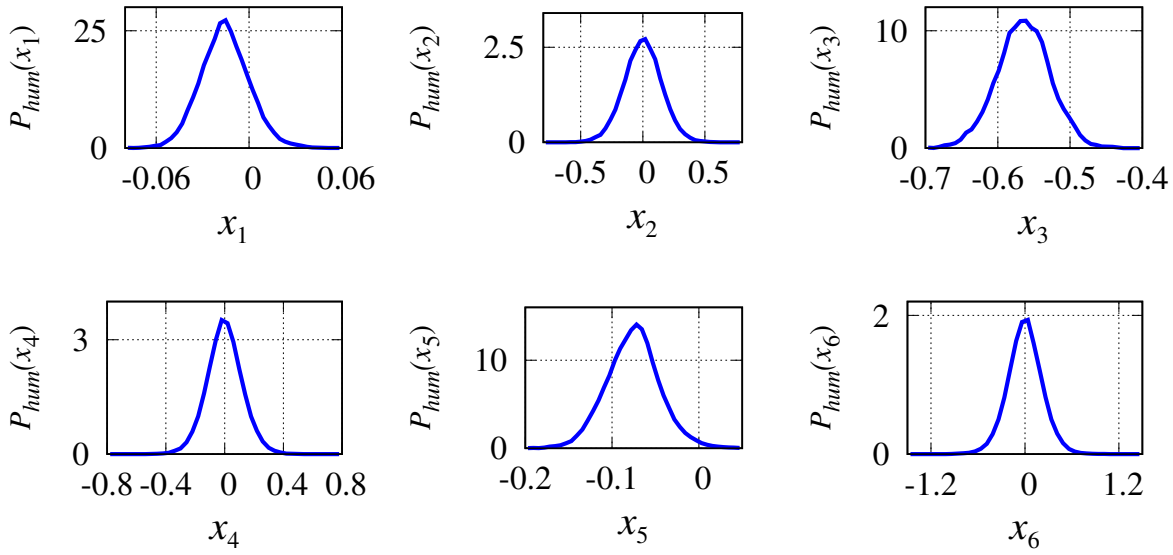

Fig. 4: The measured PDFs from the third participant ($s = 3$).

Table 1: The mean values of roll angle, wheel's lateral displacement, and steering angle for the sth participant.

k	1	3	5
$E^{(1)}[x_k]$	-1.07×10^{-2}	-5.72×10^{-1}	-1.01×10^{-1}
$SD^{(1)}[x_k]$	1.88×10^{-2}	3.68×10^{-2}	3.30×10^{-2}
$E^{(2)}[x_k]$	-1.86×10^{-3}	-6.51×10^{-1}	-1.60×10^{-1}
$SD^{(2)}[x_k]$	2.39×10^{-2}	3.30×10^{-2}	3.99×10^{-2}
$E^{(3)}[x_k]$	-1.56×10^{-2}	-5.64×10^{-1}	-7.59×10^{-2}
$SD^{(3)}[x_k]$	1.61×10^{-2}	3.70×10^{-2}	3.12×10^{-2}

of the kth component $\{x_k^{(s,n)}(t_i)\}_{i=0}^{I-1}$ with bin width $(\overline{x_k} - \underline{x_k})/N_{\rm bin}$. Here, $N_{\rm bin}$ is the number of histogram bins and $\overline{x_k}$ and $\underline{x_k}$ are the upper and lower limits of x_k, respectively. The resulting $P_{hum}^{(s,n)}(x_k)$ is averaged over all trials to obtain the sth participant's PDF as

$$P_{hum}^{(s)}(x_k) = \frac{1}{N}\sum_{n=1}^{N} P_{hum}^{(s,n)}(x_k), \quad k = 1, \cdots, 6. \tag{3}$$

We call (3) the measured PDF of the sth participant.

Figure 4 shows the measured PDF of the third participant ($s = 3$). In this way, we obtained the measured PDFs for all $s = 1, \cdots, S$. In this study, we commonly set $N_{\rm bin} = 40$ while $\overline{x_k}$ and $\underline{x_k}$ are chosen for each participant, to make them cover the respective distribution of the experimental time series.

As shown in Figure 4, the vibrational centers (peaks) of $x_1 := \theta$, $x_3 := y$, and $x_5 := \phi$ are shifted from their origins, $\theta = 0$, $y = 0$, and $\phi = 0$. This is because these calibrated origins do not indicate the physical centers of human-bicycle motions, as mentioned in Section 2.2.

We statistically evaluate these shifts by their means:

$$E^{(s)}[x_k] := \frac{1}{N \times I}\sum_{n=1}^{N}\sum_{i=0}^{I-1} x_k^{(s,n)}(t_i), \quad s = 1, \cdots, S, \quad k = 1, 3, 5, \tag{4}$$

which is the temporal average of the sth participant's $\theta(t)$, $y(t)$, and $\phi(t)$ further averaged over all of his trials. Thus, we have the approximation of the shifts as

$$(\hat{\theta}, \hat{y}, \hat{\phi}) \approx (E^{(s)}[x_1], E^{(s)}[x_3], E^{(s)}[x_5]), \tag{5}$$

where $\hat{\theta}$, $\hat{y}$, and $\hat{\phi}$ are the shifts of $\theta(t)$, $y(t)$, and $\phi(t)$, respectively. The resulting values are listed in Table 1 with standard deviations given by

$$SD^{(s)}[x_k] = \sqrt{V^{(s)}[x_k]},$$
$$V^{(s)}[x_k] := \frac{1}{N \times I - 1}\sum_{n=1}^{N}\sum_{i=0}^{I-1}\left(x_k^{(s,n)}(t_i) - E^{(s)}[x_k]\right)^2, \quad s = 1, \cdots, S, \quad k = 1, 3, 5. \tag{6}$$

The resulting $E^{(s)}[x_k]$ ($k = 1, 3, 5$) values in Table 1 are slightly different as they depend on the respective riding forms of the participants.

3 Human fluctuation model

3.1 A human-bicycle fluctuation model

We model the human bicycle mechanics by a carted inverted pendulum. Based on the time series statistics in Table 1, we also assume that the roll angle

θ about the equilibrium and steering angle ϕ about the straight running is sufficiently small; the maximal three standard deviation indicates $3\times\max_s SD^{(s)}[x_1] \approx 7.17\times10^{-2}$ rad (or 4.10° deg). $3\times\max_s SD^{(s)}[x_5] \approx 1.19\times10^{-1}$ rad (or 6.81° deg). Therefore, we model the bicycle's motion by a linearized carted inverted pendulum of the form:

$$\begin{cases} \ddot{y}+\ddot{\theta}-g(\theta-\hat{\theta})+c_\theta\dot{\theta}=0, \\ \ddot{y}+c_y\dot{y}+c_\phi\dot{\phi}=V\dot{\phi}, \end{cases} \tag{7}$$

where $g := 9.81$ m/s^2 is gravitational acceleration, c_θ, c_y, and c_ϕ are viscous dampings, and V is a bicycle speed. The equation of motion (7) is nondimensionalized and represented in the following state-space form:

$$\begin{cases} \dot{x}_1 = x_2, \\ \dot{x}_2 = -Vx_6 + c_y x_4 + g(x_1-\hat{\theta}) - c_\theta x_2, \\ \dot{x}_3 = V(x_5-\hat{\phi}), \\ \dot{x}_4 = Vx_6 - c_y x_4 - c_\phi x_6, \\ \dot{x}_5 = x_6, \\ \dot{x}_6 = u(t), \end{cases} \tag{8}$$

where $u(t)$ is a human input.

The human input $u(t)$ is specified to simulate the human fluctuation during human-bicycle motion. As successfully demonstrated in our previous study [5, 6], some human fluctuations can be accurately simulated by the following state-feedback mechanism:

$$\begin{aligned} u(t) = {} & F_1(x_1-\hat{\theta}) + F_2x_2 + F_3(x_3-\hat{y}) + F_4x_4 \\ & + \mu(1+\sigma_1\xi_1)(x_5-\hat{\phi}) + F_6x_6 + \sigma_2\xi_2. \end{aligned} \tag{9}$$

Here, F_1 and F_3 are the deterministic proportional gains of the roll angle and the wheel's lateral displacement, respectively. F_2, F_4, and F_6 are the deterministic derivative gains of the roll angle, the wheel's lateral displacement, and the steering angle, respectively. $\xi_1(t)$ and $\xi_2(t)$ are independent white Gaussian noises with zero mean and unit variance. σ_1 and σ_2 are multiplicative and additive noise strengths, respectively. Thus, $\mu(1+\sigma_1\xi_1)$ represents a random proportional gain with mean μ and variance $(\mu\sigma_1)^2$ and $\sigma_2\xi_2(t)$ represents an additive random perturbation.

Finally, we substitute (9) into (8) and obtain our proposed human-bicycle fluctuation model, with the generalized parameter vector:

$$\begin{aligned} \boldsymbol{p} &= (p_1,\cdots,p_{11}) \in \mathbb{R}^5\times\mathbb{R}^3_{\geqq 0}\times\mathbb{R}^3 \\ &:= (F_1,F_2,F_3,F_4,F_6,c_\theta,c_y,c_\phi,\mu,\sigma_1,\sigma_2), \end{aligned} \tag{10}$$

which parameterizes the human-bicycle motion properties.

3.2 Calculation of simulated PDFs

Using given $\boldsymbol{q} := (\hat{\theta},\hat{y},\hat{\phi})$ and $\boldsymbol{p}$, we obtain N' samples of the stationary numerical solution of (8) and (9) as

$$\{\boldsymbol{x}_A^{(n')}(t_i;\boldsymbol{q},\boldsymbol{p})\}_{i=0}^{I-1}, \quad n'=1,\cdots,N', \tag{11}$$

by means of a fourth-order Runge–Kutta–Gill method with time step $\Delta t = 10^{-2}$ s. To generate these samples, N' different sequences of normal pseudo-random numbers:

$$\{\nu_i^{(n')}\}_{i=0}^{I-1}, \quad n'=1,\cdots,N' \tag{12}$$

are used to simulate the independent white Gaussian noises $\xi_1(t)$ and $\xi_2(t)$ by

$$\xi_l(t_i) \approx \nu_i^{(n')}(\Delta t)^{-1/2}, \quad l=1,2, \tag{13}$$

where $(\Delta t)^{-1/2}$ is the numerical factor required for integrating stochastic differential equations [10].

From the kth component of the simulated time series in (11), we construct the n'th sample's PDF $P_{sim}^{(n')}(x_k;\boldsymbol{q},\boldsymbol{p})$ using the same procedure and conditions as applied for deriving the measured PDF in Section 2.3. We also take the average $P_{sim}^{(n')}(x_k;\boldsymbol{q},\boldsymbol{p})$ over all samples by

$$P_{sim}(x_k;\boldsymbol{q},\boldsymbol{p}) = \frac{1}{N'}\sum_{n'=1}^{N'} P_{sim}^{(n')}(x_k;\boldsymbol{q},\boldsymbol{p}), \quad k=1,\cdots,6. \tag{14}$$

We call (14) the simulated PDFs for $\boldsymbol{q}$ and $\boldsymbol{p}$, which are to be compared with the measured $P_{hum}^{(s)}(x_k)$.

4 Method of parameter identification

We identify the parameter vector $\boldsymbol{p}$ by which the simulated $P_{sim}(x_k;\boldsymbol{q},\boldsymbol{p})$ reproduces the measured $P_{hum}^{(s)}(x_k)$, $k=1,\cdots,6$, by solving the optimization problem:

$$\underset{\boldsymbol{p}}{\text{Minimize}}\, E(\boldsymbol{p}) \tag{15}$$

with the cost function

$$\begin{aligned} E(\boldsymbol{p}) &:= \sum_{k=1}^{6} a_k E_k(\boldsymbol{p}), \quad a_k>0, \\ E_k(\boldsymbol{p}) &:= \frac{\int_{\underline{x_k}}^{\overline{x_k}}\{P_{sim}(x_k;\boldsymbol{q},\boldsymbol{p})-P_{hum}^{(s)}(x_k)\}^2dx_k}{\int_{\underline{x_k}}^{\overline{x_k}}\{P_{hum}^{(s)}(x_k)\}^2dx_k}. \end{aligned} \tag{16}$$

Here, a_k are weight coefficients and $E_k(\boldsymbol{p})$ is the integral of the SRs between the simulated $P_{sim}(x_k;\boldsymbol{q},\boldsymbol{p})$ and the measured $P_{hum}^{(s)}(x_k)$, as normalized by the integral of the squared $P_{hum}^{(s)}(x_k)$. Therefore, this cost function evaluates the PDF's reproduction error and satisfies $E(\boldsymbol{p})=0$ if $P_{sim}(x_k;\boldsymbol{q},\boldsymbol{p}) = P_{hum}^{(s)}(x_k)$, $k=1,\cdots,6$.

In this study, we employed PSO [11] to solve (15), with 2048 particles and 500 iterations. The initial particles $\boldsymbol{p}^i(0)$, $i=1,\cdots,M$ were given by random points uniformly distributed within the eleven-dimensional hyperrectangle: $-30\leq p_1\leq 0,\ 0\leq p_2\leq 10,\ -30\leq p_3\leq 0,\ 0\leq p_4\leq 30,\ -30\leq p_5\leq 0,\ 0\leq p_6\leq 15,\ 0\leq p_7\leq 10,\ 0\leq p_8\leq 3,\ 0\leq p_9\leq 10,\ 0\leq p_{10}\leq 20,\ 0\leq p_{11}\leq$

5. The weights were empirically set to $a_k = 1$ for all k by which the cost values were converged within the 500 iterations and the proper fitness was obtained as described below.

5 Identification results

We hereafter denote by $\boldsymbol{p}^{(s)}$ and $\boldsymbol{q}^{(s)}$ the amounts obtained from the sth participant's data. We also use the notation $P_{sim}^{(s)}(x_k) := P_{sim}(x_k; \boldsymbol{q}^{(s)}, \boldsymbol{p}^{(s)})$ for the simulated PDFs derived from the sth participant's data.

Table 2 lists the identified vector components of $\boldsymbol{p}^{(s)}$ by PSO for all participants $s = 1, 2, 3$ and the corresponding SR cost value $E(\boldsymbol{p}^{(s)})$. The last column indicates the cost value as a PDF fitness value by

$$F^{(s)} := \{1 - E(\boldsymbol{p}^{(s)})\} \times 100\,\%, \tag{17}$$

which indicates the accuracy of our human-bicycle fluctuation model in (8) and (9) in terms of the reproducibility of PDFs. The best and worst results are indicated by "**" and "*," respectively.

The results clearly show that our proposed model in (8) and (9) successfully achieved over 97% PDF fitness, even in the worst case ($s = 3$).

In Figure 5, the red small circles indicate our simulated $P_{sim}^{(s)}(x_k)$ ($k = 1, \cdots, 6$) for (a) the best case ($s = 2$) and (b) the worst case ($s = 3$). The blue solid curves indicate the corresponding $P_{hum}^{(s)}(x_k)$ measurements.

As already indicated by the PDF fitness values in Table 2, our simulated PDFs mostly agree with the measured PDFs even in the worst case ($s = 3$). The best case ($s = 2$) is in good agreement with the measured PDFs. Therefore, our proposed three DOF model fairly reproduced the PDFs of human bicycle motions.

6 Conclusion

In this study, we have constructed a three DOF human-bicycle fluctuation model that reproduces the PDFs of the experimentally measured human-bicycle balance motions.

We obtained the measured PDFs with respect to the roll angular displacement, wheel's lateral displacement, steering angular displacement, and each velocity. Using these PDFs as the training data, we identified the model parameters by PSO, minimizing the SR between the measured PDF from the participant and the simulated PDF by our model. The resulting PDF fitnesses were over 97%, indicating that the simulated PDFs reproduced the measured ones.

The above results leads to the conclusion that our proposed model can provide a three DOF fluctuation model of human-bicycle fluctuations.

In future work, we plan to predict the bicycle's running paths based on our proposed model and develop a new technology to reduce the bicycle accidents.

Acknowlegement

We wish to express our gratitude to the members of the System Dynamics Laboratory at Utsunomiya University for their participation and cooperation as participants in this study. This work was funded by JSPS KAKENHI Grant Number JP18H01391.

References

[1] Japan National Police Agency, "Traffic accident statistics annual report." `https://www.e-stat.go.jp/en/stat-search/files?lid=000001223644`, February 2019. Accessed: 2019-03-11.

[2] "Google self-driving car project monthly report." `https://www.google.com/selfdrivingcar/files/reports/report-1016.pdf`, June 2016. Accessed: 2019-03-11.

[3] J.J. Collins and C.J. De luca: *Random walking during quiet standing*, Physical Review Letters, 73–5, 764/767 (1994).

[4] J.L. Cabrera and J.G. Militon: *On-off intermittency in a human balancing task*, Physical Review Letters, 89–15, 158702:1/4 (2002).

[5] S. Matsumoto, K. Yoshida, and M. Sekikawa: *Stochastic dynamic modeling of human visuomotor tracking task of an unstable virtual object*, Transactions of the Institute of Systems, Control and Information Engineers, 31–6, 209/219 (2018).

[6] K. Yoshida, K. Sato, and Y. Yamanaka: *Simple degree-of-freedom modeling of the random fluctuation arising in humanbicycle balance*, Applied Sciences, 9–10, 2154 (2019).

[7] J.D.G. Kooijman, J.P. Meijaard, J.M. Papadopoulos, A. Ruina, and A.L. Schwab: *A bicycle can be self-stable without gyroscopic or caster effects*, Science, 332–6027, 339/342 (2011).

[8] J. Tan, Y. Gu, C.K. Liu, and G. Turk: *Learning bicycle stunts*, ACM Trans. Graph., 33–4, 50:1/50:12 , July 2014.

[9] J. Randløv and P. Alstrøm: *Learning to drive a bicycle using reinforcement learning and shaping*, Proceedings of the Fifteenth International Conference on Machine Learning, ICML '98, San Francisco, CA, USA, 463/471 , Morgan Kaufmann Publishers Inc. (1998).

[10] D.J. Higham.: *An Algorithmic Introduction to Numerical Simulation of Stochastic Differential Equations*, SIAM Review, 43–3, 525/546 (2012).

Table 2: Identified $\boldsymbol{p}^{(s)}$ and its cost value for the sth participant. "**" denotes the best result and "*" the worst.

s	p_1	p_2	p_3	p_4	p_5	p_6		
1	54.28647	14.61676	4.156761	18.44603	5.104233	9.158946		
2	57.28823	7.932240	2.008461	15.50420	1.911434	6.228664		
3	26.99948	10.64740	1.428514	6.469611	3.570648	10.08310		
s	p_7	p_8	p_9	p_{10}	p_{11}	$E(\boldsymbol{p}^{(s)})$	PDF fitness	
1	12.61928	10.45926	36.59455	0.8424895	1.766464	1.510×10^{-2}	98.49%	
2	9.352436	8.206091	12.56037	0.1545174	0.9200015	8.749×10^{-3}	99.12%	**
3	10.95418	10.43443	10.18957	1.241405	0.5660814	2.924×10^{-2}	97.07%	*

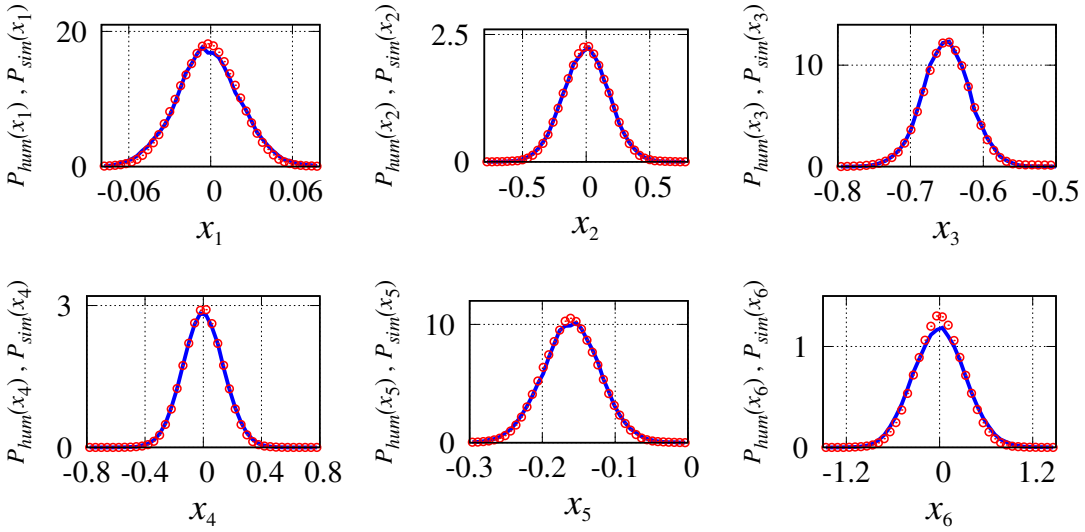

(a) The best case ($s = 2$)

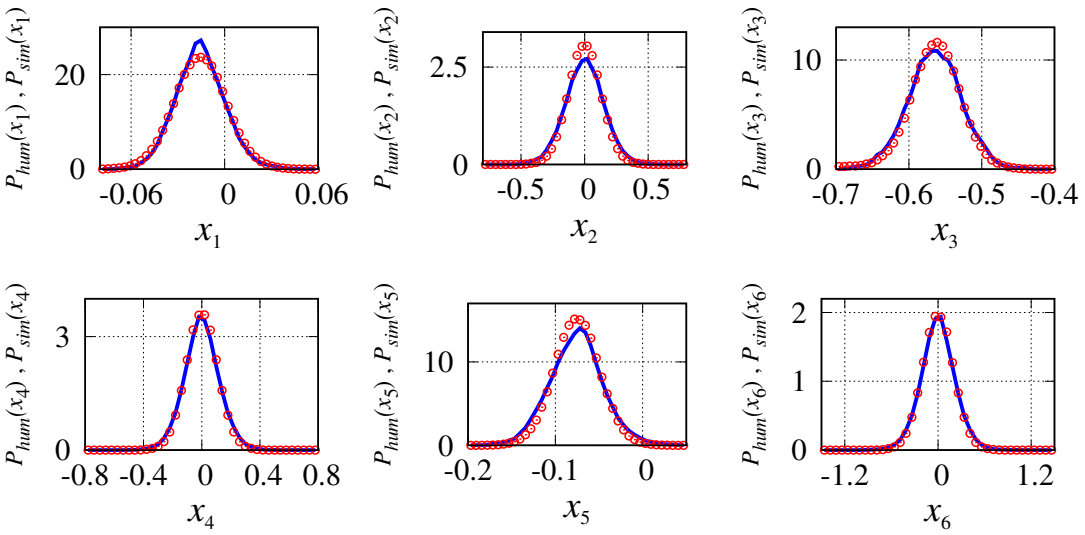

(b) The worst case ($s = 3$)

Fig. 5: Comparison between the measured $P_{hum}^{(s)}(x_k)$ and the simulated $P_{sim}^{(s)}(x_k)$, $k = 1, \cdots, 6$, for (a) the best case ($s = 2$) and (b) the worst case ($s = 3$). The blue solid curves indicate the measured PDFs and the red small circles indicate the simulated PDFs.

[11] Y. Shi and R. Eberhart: *A modified particle swarm optimizer*, 1998 IEEE International Conference on Evolutionary Computation Proceedings. IEEE World Congress on Computational Intelligence, Anchorage, AK, USA, 69/73 , IEEE, may 1998.